INSTRUMENTATION AND MEASUREMENT

Three-dimensional color particle image velocimetry based on a cross-correlation and optical flow method

Liang Shan(单良)[1,†], Jun-Zhe Xiong(熊俊哲)[1,†], Fei-Yang Shi(施飞杨)[1], Bo Hong(洪波)[1], Juan Jian(简娟)[1], Hong-Hui Zhan(詹虹晖)[1], and Ming Kong(孔明)[2,‡]

[1] *Key Laboratory of Electromagnetic Wave Information Technology and Metrology of Zhejiang Province, College of Information Engineering, China Jiliang University, Hangzhou* 310018, *China*

[2] *College of Metrology & Measurement Engineering, China Jiliang University, Hangzhou* 310018, *China*

(Received 5 September 2022; revised manuscript received 2 December 2022; accepted manuscript online 11 January 2023)

Rainbow particle image velocimetry (PIV) can restore the three-dimensional velocity field of particles with a single camera; however, it requires a relatively long time to complete the reconstruction. This paper proposes a hybrid algorithm that combines the fast Fourier transform (FFT) based co-correlation algorithm and the Horn–Schunck (HS) optical flow pyramid iterative algorithm to increase the reconstruction speed. The Rankine vortex simulation experiment was performed, in which the particle velocity field was reconstructed using the proposed algorithm and the rainbow PIV method. The average endpoint error and average angular error of the proposed algorithm were roughly the same as those of the rainbow PIV algorithm; nevertheless, the reconstruction time was 20% shorter. Furthermore, the effect of velocity magnitude and particle density on the reconstruction results was analyzed. In the end, the performance of the proposed algorithm was verified using real experimental single-vortex and double-vortex datasets, from which a similar particle velocity field was obtained compared with the rainbow PIV algorithm. The results show that the reconstruction speed of the proposed hybrid algorithm is approximately 25% faster than that of the rainbow PIV algorithm.

Keywords: particle image velocimetry, color light, cross-correlation and optical flow method, vortex

PACS: 47.80.Cb, 47.54.De, 47.80.Jk **DOI:** 10.1088/1674-1056/acb1ff

1. Introduction

Fluid movement exists widely in nature and in the chemical industry, aerospace, hydropower, combustion and other industrial fields, such as in burning flames,[1] river flow, turbulent flow in the atmosphere[2] and fluids in industrial pipes. In 1904, Prandtl observed fluid motion at the boundary layer using micro-particle flow visualization through the hand-shaking flume experiment, which started a chapter of scientific research on fluid motion.

Particle image velocimetry (PIV) is a transient, multipoint, contactless hydrodynamic velocimetry method that can accurately measure the transient flow field in the plane and visualize the flow field structure. It provides an excellent data basis for the qualitative description of and quantitative research into fluid motion without disturbing the fluid motion.[3,4] In the past 20 years, many typical three-dimensional (3D) PIV techniques have been developed, among which stereoscopic PIV (stereo PIV)[5–7] and tomographic PIV (tomo PIV)[8–10] are representative and widely used techniques. In stereo PIV, two cameras are set at a certain angle to shoot the same area to be measured. Furthermore, the two-dimensional (2D) velocity field can be obtained by cross-correlating the image, and the 3D velocity is calculated by the projection reconstruction method based on the motion information of the particles extracted from the two views outside the imaging plane.[11] Calluaud and David discussed the advantages of stereo PIV technology and the accuracy of the back-projection algorithm, established the transformation relationship between the natural object and the image coordinates during 3D reconstruction and evaluated the accuracy of the algorithm reconstruction by the magnitude of the angular displacement.[12] Stereo PIV is often used to measure liquid flow and in industrial wind tunnels.[13]

Elsinga and colleagues proposed tomo PIV for the first time in 2006.[14] Tomo PIV has a similar structure to stereo PIV; however, tomo PIV requires restoration of the 3D particle field from the 2D particle image through the optical tomography algorithm before restoring the velocity field. The 3D motion information for the flow field is obtained by analyzing and reconstructing the 3D particle field using the 3D cross-correlation algorithm. In 2013, De Silva *et al.* optimized tomo PIV using image matching reconstruction technology to improve the reconstruction accuracy of the algorithm.[15] In 2019, Qu *et al.* proposed a method to reconstruct the 2D velocity distribution of flow fields by laser absorption spectroscopy tomography, which does not require extra tracer particles and avoids issues arising from the short lifetime of molecular tags.[16] In 2021, Zhang *et al.* combined the meshless radial

[†]These authors contributed equally to this work.

[‡]Corresponding author. E-mail: mkong@cjlu.edu.cn

© 2023 Chinese Physical Society and IOP Publishing Ltd

basis function (RBF) method with modified Tikhonov regularization to solve severely ill-posed and underdetermined acoustic tomography problems.[17] Although tomo PIV has a higher reconstruction accuracy than stereo PIV, it requires multiple cameras to photograph particles in the flow field from different angles to obtain 3D velocity information. The experimental setup of actual tomo PIV is generally complicated due to the placement and shooting angles of multiple cameras, which is a grave limitation in actual fluid measurements.[18] Light-field PIV (LF-PIV) has become a research hotspot in recent years. Zhu *et al.* studied the volumetric resolution of light-field imaging and its effect on the reconstruction of LF-PIV, and determined the proper particle concentration for practical LF-PIV experiments.[19] In 2021, Zhu *et al.* made improvements to LF-PIV, and proposed a pre-recognition simultaneous algebraic reconstruction technique (SART) algorithm for the volumetric reconstruction of LF-PIV that is capable of mitigating the elongation effects of the reconstructed tracer particles at different depths and improving the measurement accuracy of the instantaneous velocity field.[20] However, the computational efficiency of LF-PIV is not so high.

PIV based on color illumination is a novel 3D PIV reconstruction algorithm that encodes the depth positions of particles in the 3D fluid using different colors. Combined with the 2D position information about the particles in the image, the 3D velocity field of the flow field can be reconstructed with a single camera. The experimental setup of color PIV is more straightforward, has fewer measurement limitations and is more adaptable to different real measurement environments compared with tomo PIV.[21] In 2017, Xiong *et al.* proposed rainbow PIV, which uses different colors to encode the depth information of particles.[22] An image formation model is established to reconstruct the particle distribution field, and the 3D velocity vector field is estimated by the 3D optical flow algorithm combining the image formation model and physical constraints. However, the rainbow PIV algorithm is limited by its relatively longer reconstruction time.

This work presents a cross-correlation and optical flow method for estimation of the 3D velocity field of fluid flow based on color PIV. First, an image formation model under color illumination is established, correlating the position of particles in 3D space with their imaging on the color charge-coupled device (CCD) camera. A minimization problem on particle distribution is modeled based on the image formation of particles under colored illumination. Furthermore, the alternating direction method of multipliers (ADMM) is used to obtain the 3D particle distribution probability field. The cross-correlation algorithm is used to analyze and reconstruct the probability field of 3D particle distribution at different times to obtain a rough 3D velocity estimation; this is conducted in the second iteration to improve the position estimation of particles. Finally, the Horn–Schunck (HS) optical flow algorithm is used to analyze and reconstruct the 3D particle distribution field to obtain an accurate 3D velocity field.

2. Principle and algorithm

2.1. Reconstruction of 3D particle distribution field

In an incoherent imaging system, the image intensity in the process of image formation is linear in the theoretical description of a linear system. The generated image can be considered as the sum of independent individual imaging objects. The imaging process of the optical system can be modeled as a set of point spread functions (PSFs) because incoherent light is used in the color illumination system. The PSF is divided into three color channels — red, green and blue (RGB) — depending on which corresponding point spread function $g_{\mathrm{C}}(x,\lambda)$, $C \in \{\text{red, green, blue}\}$ could be established.

The color illumination system is equipped with a continuous narrow-band uncorrelated spectral filter, the wavelength λ of which changes linearly with depth Z, to encode the position of particles in 3D space with the color of the light. The depth information for particles in 3D space can be determined by the wavelength λ of the reflected light. Particle images captured by color CCD cameras can be simulated by the light intensity distribution of particles on the image plane and the convolution sum of the PSF, as shown below:

$$i_{\mathrm{C}}(X) = \int_{\Lambda}\int_{X} g_{\mathrm{C}}\left(X - X', \lambda\right) \cdot i(X,\lambda) \cdot P(X,\lambda)\,\mathrm{d}X'\,\mathrm{d}\lambda, \quad (1)$$

where λ is the wavelength of light reflected by the tracer particle at a certain depth, $i_{\mathrm{C}}(X)$ represents a color image of particles captured by cameras with different RGB color channels and $i(X,\lambda)$ denotes the corresponding spectral distribution of particles incident on the image sensor. The spatial integral corresponds to a convolution representing a potentially imperfect focus, whereas the wavelength integral represents the conversion from a spectral image to a RGB image that encodes the 3D particle position.

A minimization problem needs to be constructed to solve the distribution field of the particles. First, the convolution formula of PSF and reflected light intensity are discretized to obtain a matrix $\boldsymbol{A} \in R^{3N\times NL}$, where N corresponds to the number of image pixels, L denotes the number of discretization levels along the wavelength coordinate and the number 3 represents three different color channels. Furthermore, $\boldsymbol{i}_t \in [0,1]^{NL}$ represents the particle image captured by the camera at time t and $\boldsymbol{p}_t \in [0,1]^{NL}$ represents the probability that the particle exists at different points at time point t. The probability distribution of the particle field at each time point can be obtained by solving the following linear system:

$$\boldsymbol{A}\boldsymbol{p}_t = \boldsymbol{i}_t. \quad (2)$$

A linear system is necessary to introduce the sparsity and motion consistency of particles as regular terms and turn the above problem into a minimization problem (see Eq. (3)) because it is an ill-conditioned inverse problem to solve[22]

$$\begin{aligned}(p^*) \;=\; & \arg\min \frac{1}{2}\left\|\boldsymbol{A}\left[\boldsymbol{p}_t \mid \boldsymbol{p}_{t+1}\right]-\left[\boldsymbol{i}_t \mid \boldsymbol{i}_{t+1}\right]\right\|_2^2 \\ & +k_1\left\|\operatorname{diag}(\boldsymbol{w})\left(\boldsymbol{p}_t ; \boldsymbol{p}_{t+1}\right)\right\|_1+\Pi_{[0,1]}\left(\boldsymbol{p}_t ; \boldsymbol{p}_{t+1}\right) \\ & +k_2 \sum_{t=1}^{T} \int_{\Omega} \boldsymbol{p}_t \odot\left(\boldsymbol{p}_t-\boldsymbol{p}_{t+1}\left(\boldsymbol{u}_t,-\Delta t\right)\right)^{\circ 2} \mathrm{d} \Omega, \quad (3)\end{aligned}$$

where $\odot$ is the Hadmard product operator and $(\cdot)^{\circ 2}$ denotes the Hadmard square operator. The operator $\Pi_{[0,1]}$ projects the probability of the existence of particles in all 3D spaces onto the effective probability $[0,1]^{NL}$.

Due to the weighting matrix and index function, the above-mentioned optimization problem of the particle distribution field is non-smooth. The proximal gradient and ADMM methods are both commonly used to solve non-smooth problems. The ADMM algorithm has a better performance than the proximal gradient method, and is chosen in this study (Algorithm 1).[23,24] When the ADMM algorithm solves the particle distribution field,[25,26] the minimization problem is decomposed into two local minimization problems F_1 and H_1, and the two objective functions are iteratively solved to obtain the 3D distribution field of the particles

$$\begin{aligned}F_1(p) \;=\; & \frac{1}{2}\left\|\boldsymbol{A}\left[\boldsymbol{p}_t \mid \boldsymbol{p}_{t+1}\right]-\left[\boldsymbol{i}_t \mid \boldsymbol{i}_{t+1}\right]\right\|_2^2 \\ & +k_2 \sum_{t=1}^{T} \int_{\Omega} \boldsymbol{p}_t \odot\left(\boldsymbol{p}_t-\boldsymbol{p}_{t+1}\left(\boldsymbol{u}_t,-\Delta t\right)\right)^{\circ 2} \mathrm{d} \Omega, \quad (4) \\ H_1(p) \;=\; & \mathrm{k}_1\left\|\operatorname{diag}(\boldsymbol{w})\left(\boldsymbol{p}_t ; \boldsymbol{p}_{t+1}\right)\right\|_1+\Pi_{[0,1]}\left(\boldsymbol{p}_t ; \boldsymbol{p}_{t+1}\right). \quad (5)\end{aligned}$$

The corresponding near-end operators $\operatorname{prox}_{\sigma_1 F_1}$ and $\operatorname{prox}_{\tau_1 H_1}$ are used to minimize the objective functions F_1 and H_1

$$P=\operatorname{prox}_{\sigma_1 F_1}\left(z^j-q^j\right) \Rightarrow \boldsymbol{\sigma}_1 \boldsymbol{A}^T \boldsymbol{i}_1+z^j-q^j, \quad (6)$$

$$\Pi_{[0,1]}\left(\left(e^j-\tau_1 k_1 \boldsymbol{w}\right)_+-\left(-e^j-\tau_1 k_1 \boldsymbol{w}\right)_+\right). \quad (7)$$

In Eq (6), P is represented by the procedural operator and is solved by conjugate gradients. Equation (7) is the point-wise shrinkage operation followed by a projection onto the domain of [0,1].

Algorithm 1. Reconstruction process of the particle distribution field using the ADMM algorithm.

1. Input objective function F_1, H_1
2. Set the number of iterations j, the relaxation variable z, the maximum number of iterations max
3. Initialize the particle distribution probability p
4. for $j=1:\max$
5. //Minimize p by proximal operator $\operatorname{prox}_{\sigma_1 F_1}$ based on F_1
6. $p^{j+1} \leftarrow \operatorname{prox}_{\sigma_1 F_1}\left(z^j-q^j\right)$
7. //Minimize z by proximal operator $\operatorname{prox}_{\tau_1 H_1}$ based on H_1
8. $z^{j+1} \leftarrow \operatorname{prox}_{\tau_1 H_1}\left(p^{j+1}-q^j\right)$
9. //Update the dual variable q according to the reduced variables p^{j+1} and z^{j+1}
10. $q^{j+1} \leftarrow q^j+p^{j+1}-z^{j+1}$
11. end
12. Output the particle distribution probability field

2.2. Reconstruction of 3D velocity field

The cross-correlation algorithm has the advantages of a simple principle and relatively easy computation. However, because the velocity vector reconstructed by the cross-correlation algorithm is the average displacement of all particles in the interrogation window, it cannot achieve high-resolution velocity field reconstruction. Therefore, it is not suitable for reconstructing the velocity field of a micro-scale flow field.[27] The optical flow method can reconstruct the fluid velocity field at the single-pixel level, which is better than the cross-correlation algorithm in resolution. The optical flow method originates from the theory of computer vision. The corresponding objective function should be constructed assuming luminance consistency and spatial consistency. Then, the gradient descent algorithm is used to minimize the objective function to obtain the fluid velocity field. However, minimization in the optical flow method often requires multiple iterations and variational optimization, which will lead to low computational efficiency and a long reconstruction time.[28]

This study combined the cross-correlation algorithm and the optical flow method. The FFT-based cross-correlation algorithm was used to quickly solve the rough velocity field, all of which were used as the regular term of the particle motion consistency when the ADMM algorithm reconstructed the particle field to obtain an accurate particle distribution field. Finally, the HS optical flow algorithm based on physical constraints was used to conduct pyramid iterations on the particle distribution field to obtain a high-resolution 3D velocity field. Figure 1 shows a block diagram of the cross-correlation and optical flow method.

First, the PSF of particles in 3D space at different depths is set, and two digital particle images taken at different times I_1 and I_2 are input. Then, the digital particle images are filtered using a Gaussian filter, and the resolution of the digital particle images can be obtained. The matrix $\boldsymbol{A}$ in the system linear equation and the weighting term $\boldsymbol{w}$ of the sparse particle

distribution will be obtained according to the image size and the PSF matrix.

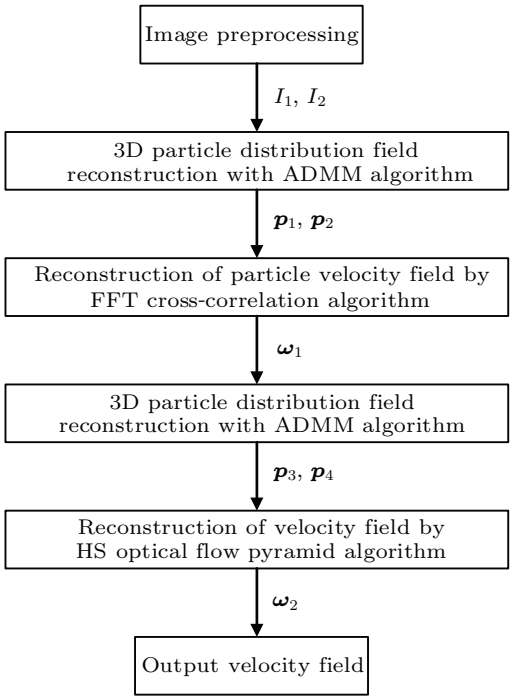


Fig. 1. Block diagram of 3D color PIV based on the cross-correlation and optical flow method.

When the coefficient k_2 of the particle motion consistency regularization term is 0, the problem of minimizing particle distribution can be solved by the ADMM algorithm to obtain the 3D particle distribution probability fields $\boldsymbol{p}_1$ and $\boldsymbol{p}_2$, i.e., the probability that a particle exists at a point.

The average speed of the particles can be calculated because the time interval Δt of image acquisition can be obtained by setting the hardware device. However, the amount of calculation needed for the two-dimensional product sum operation and the time required for the CPU operation were very large based on the definition of cross-correlation to solve the motion velocity of the flow field directly. The one-dimensional time complexity of the direct cross-correlation analysis of the fluid velocity was $O(N^2)$; therefore, the amount of calculation required for cross-correlation increases rapidly with increasing sequence length. The cross-correlation algorithm based on FFT (FFT-CC) was used to improve the efficiency for initially estimating the velocity field of the fluid, saving the time consumed by the complex integral calculation; the computational complexity was $O(N\log_2 N)$. The amount of calculation was reduced significantly, and the real-time performance of PIV measurement was improved compared with the complexity $O(N^2)$ of the conventional cross-correlation algorithm. The FFT-CC algorithm was used to quickly solve the probability fields of the two-particle distributions obtained above; the anomalies in the velocity fields were detected based on the basic principles of hydrodynamics, and the local median method was used to correct the anomalous vectors to obtain a rough velocity estimate $\boldsymbol{\omega}_1$.

The coefficient k_2 of the particle motion consistency regularization term in the objective function for minimizing the particle distribution was then set to 1, and the rough velocity estimation obtained by the cross-correlation algorithm based on FFT was used as prior knowledge of the particle distribution to minimize the objective function. The ADMM algorithm was used to optimize the solution of the minimization problem to obtain accurate particle distribution probability fields $\boldsymbol{p}_3$ and $\boldsymbol{p}_4$. Values with probabilities less than 0.01 in $\boldsymbol{p}_3$ and $\boldsymbol{p}_4$ matrices were regarded as errors and should be eliminated. Hence, a 3D particle distribution field was obtained.

Algorithm 2 gives the accurate particle distribution field obtained after the second iteration, the high-resolution 3D velocity field $\boldsymbol{\omega}_2$ using the HS optical flow pyramid algorithm based on physical constraints and the process for solving optical flow method.

Algorithm 2. Reconstruction process of particle velocity field using HS optical flow algorithm.

1. Input image pair Img_1 and Img_2
2. Set weight factor λ
3. Image preprocessing (Gaussian filtering)
4. Generate image pyramid: layer 0 to layer L
5. for $l = L$ to 0 do
6. if $l = L$ then
7. Initialize the velocity field $\boldsymbol{\omega}_{l+1}$
8. else
9. Interpolate the velocity field $\boldsymbol{\omega}_{l+1}$ of the previous layer to obtain the velocity field $\hat{\boldsymbol{\omega}}_{l+1}$
10. end
11. a. Symmetrical deformation of images
12. b. Solving the velocity field according to the ADMM optimization framework
13. c. Filter the velocity field to detect outliers and remove them
14. d. Enter the next level pyramid
15. end
16. Output velocity field

3. Simulation and analysis

3.1. Single-vortex velocity field reconstruction

Single-vortex simulation experiments were performed to verify and analyze the performance of the proposed method. Five hundred particles in a 3D space of 72 pixels×120 pixels×20 pixels were randomly generated. The color particle image I_1 at time t_1 was obtained based on the particle imaging model. Then, a single vortex with a maximum speed of 5 pixels·s^{-1} was simulated in the 3D space depending on the flow field model. In the core Rankine vortex, the center coordinate of the vortex core was [60, 36] and the core radius of the vortex was 30 pixels. The 3D coordinates of particles at time t_2 were predicted using the simulated vortex, and the digital color particle image I_2 was obtained by simulating imaging.

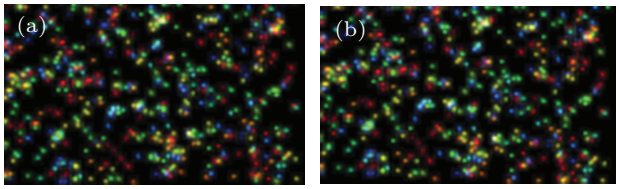


Fig. 2. Single vortex simulation image: (a) color particle image I_1 at time t_1; (b) color particle image I_2 at time t_2.

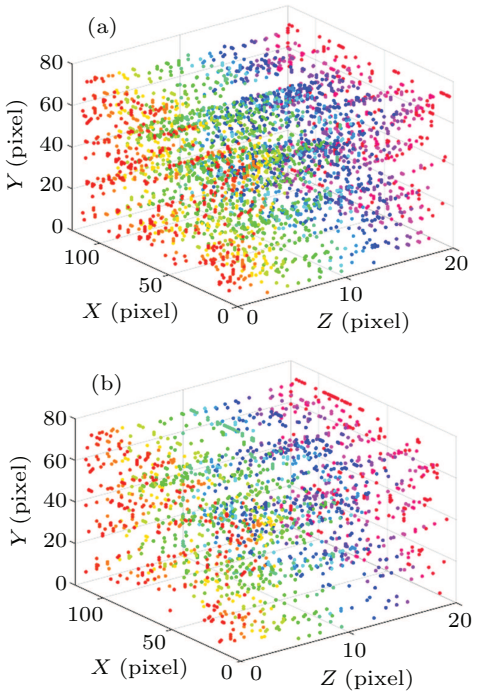


Fig. 3. Visualization of 3D particle distribution: (a) 3D particle distribution at time t_1; (b) 3D particle distribution at time t_2.

An objective minimization function about the probability of particle distribution was constructed according to the PSF of particles at different depths and the resolution of the color particle image. The ADMM algorithm was used to solve the minimization problem to obtain the 3D distribution probability field of particles. The 3D matrices $\boldsymbol{p}_1$and $\boldsymbol{p}_2$ represent the probability of particles in each position in 3D space, with a size of 72 pixels×120 pixels×20 pixels. When the value in the probability field of 3D particle distribution was greater than 0.5, the particle was considered to exist. Particles at different depths were marked with different colors, as shown in Fig. 3.

According to the 3D distribution fields $\boldsymbol{p}_1$ and $\boldsymbol{p}_2$ of the particles, the FFT-CC algorithm was used to reconstruct the rough 3D velocity field. The size of the detection window was set to be 8×8×8. Furthermore, $\boldsymbol{p}_1$ and $\boldsymbol{p}_2$ were meshed, and cross-correlation analysis was performed for each detection window. After that, a three-layer pyramid with coarse-to-fine resolution was constructed by down sampling and Gaussian low-pass filtering. The bottom-up particle distribution field resolutions were 72×120×20, 36×60×20 and 18×30×20, respectively. Furthermore, the pyramid HS optical flow algorithm was used to analyze and reconstruct the accurate 3D particle velocity field. Finally, the high-resolution 3D particle velocity field was obtained as the output, shown in Fig. 4.

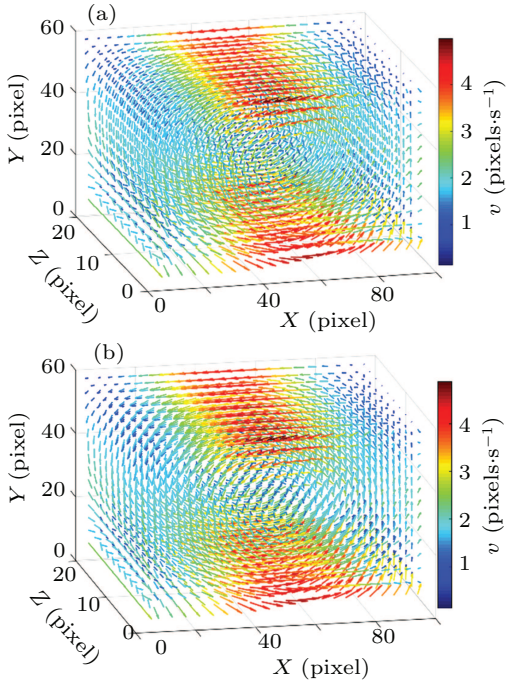


Fig. 4. Accurate 3D particle velocity field: (a) rainbow PIV algorithm; (b) proposed method.

The reconstruction performance of the proposed algorithm was compared with that of the rainbow PIV algorithm. The average endpoint error (AEPE) and average angular error (AAE) of all the velocity vectors were used to evaluate the accuracy of the reconstruction. The time required to reconstruct the 3D velocity field was recorded simultaneously. The calculation formulae for AEPE and AAE are

$$\mathrm{AEPE} = \frac{\sum_{s\in c_1} \arccos\left(\dfrac{\boldsymbol{W}_\mathrm{r}(s)\cdot\boldsymbol{W}_\mathrm{g}(s)}{\|\boldsymbol{W}_\mathrm{r}(s)\|\|\boldsymbol{W}_\mathrm{g}(s)\|}\right)}{N}, \tag{8}$$

$$\mathrm{AAE} = \frac{\sum_{s\in c_1} \|\boldsymbol{W}_\mathrm{g}(s) - \boldsymbol{W}_\mathrm{r}(s)\|}{N}, \tag{9}$$

where s denotes the image coordinate, $\boldsymbol{W}_{\mathrm{g}}(s)$ and $\boldsymbol{W}_{\mathrm{r}}(s)$ represent the ground-truth velocity field and the reconstructed velocity field, respectively, c_1 corresponds to the set of single-point positions in the image and N denotes the size of c_1.

Table 1 lists AEPE, AAE and the reconstruction time of the two algorithms. We can see that values of AEPE and AAE are almost equal; in other words, the two algorithms have a similar reconstruction accuracy. But it is worth mentioning that the calculation time of the proposed algorithm is 20% shorter than that of the rainbow PIV algorithm.

Table 1. Comparison of reconstruction results.

Method	AEPE (pixels)	AAE (°)	Time (s)
Rainbow RIV	0.9145	13.7762	606
Proposed	0.9147	13.7621	485

3.2. Effect of the velocity value on reconstruction results

The velocity value affected the reconstruction result when reconstructing the 3D velocity field of the fluid. Five hundred particles in a 3D space of 72 pixels×120 pixels×20 pixels were simulated to move in a single-vortex core Rankine vortex with different velocities, and five different flow field datasets were obtained. The center coordinate of the vortex and radius of the core vortex were [60, 36] and 30 pixels, respectively. Moreover, the maximum speed of the vortex was 1, 2, 3, 4 and 5 pixels·s^{-1}. The two algorithms were used to reconstruct the velocity field of five datasets, and the reconstructed velocity field was compared with the ground-truth. Table 2 shows the reconstruction results.

When measuring the Rankine vortex field with different maximum velocities, the reconstruction errors of the proposed method and the rainbow PIV algorithm were similar (see Table 2) with changing velocity. Specifically, the error AEPE of the algorithm increased gradually, while the value of AAE decreased. From the perspective of the running time, the proposed algorithm was 20% quicker than the rainbow PIV algorithm in all cases. Moreover, the time required for reconstructing simulation data sets with different speeds was approximately the same.

Table 2. Effect of velocity value on the reconstruction results.

Speed	AEPE (pixels)		AAE (°)		Time (s)	
(pixels·s^{-1})	Rainbow PIV	Proposed	Rainbow PIV	Proposed	Rainbow PIV	Proposed
1	0.2277	0.2283	23.3622	23.3612	615	465
2	0.3605	0.3640	17.5109	18.0807	626	482
3	0.5546	0.5562	14.7826	14.5812	623	492
4	0.7068	0.7069	14.3638	14.3601	623	493
5	0.9145	0.9147	13.7762	13.7621	606	485

3.3. Effect of particle density on reconstruction results

The density of the tracer particles also affects the accuracy of the reconstruction of the 3D velocity field. We randomly generated 100, 200, 300, 400 and 500 particles in a 3D space of 72 pixels×120 pixels×20 pixels. The maximum speeds generated in the 3D space were 1, 2, 3, 4 and 5 pixels·s^{-1}. The coordinates of the center of the rigid vortex and radius were [60, 36] and 30 pixels, respectively. Twenty-five simulated particle image pairs were obtained from the Rankine vortex field at the center of a single vortex. Figure 5 shows the reconstruction accuracy.

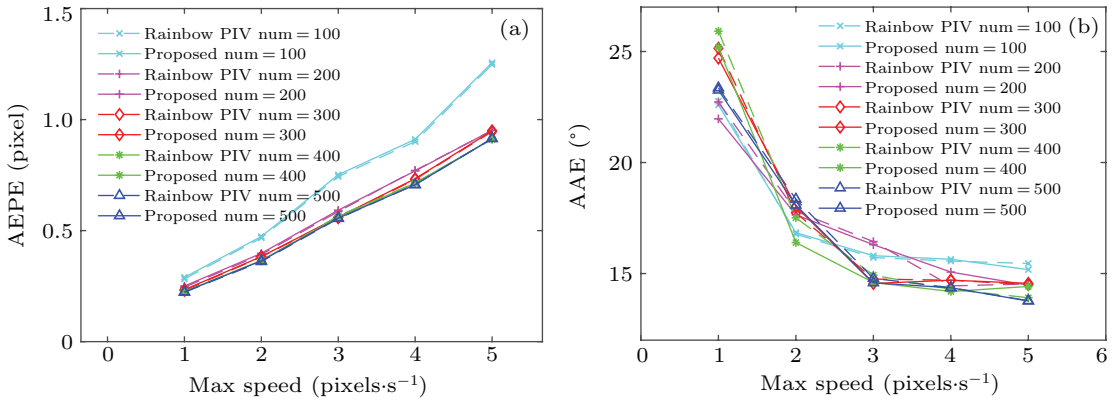


Fig. 5. Effect of velocity and particle density on reconstruction accuracy: (a) AEPE, (b) AAE.

Figure 5 shows the effect of particle velocity and density on AEPE and AAE. When particle density was the same, the value of AEPE increased with increasing velocity. It showed the same change trend for different particle densities, indicating that the reconstruction error of the hybrid algorithm increases with increasing velocity. In the vortex at the same velocity, AEPE decreased with increasing particle density. More information is available when performing 3D reconstruction

because there are more particles in the reconstructed simulated image, resulting in more accurate reconstruction results. When the particle density was constant, the angular error reconstructed by the hybrid algorithm decreased with increasing velocity. The variation trend of AAE with velocity magnitude remained the same at low and high particle concentrations, which is opposite to the variation trend for error in velocity magnitude. The larger the velocity, the smaller the change in velocity direction caused by the error, due to the same velocity error. Hence, the trend of AAE and AEPE changed with velocity.

Table 3 shows the reconstruction time of the two algorithms. From Table 3 it can be seen that the proposed method can complete the velocity field measurement in a shorter time. The calculation time gradually increased with increasing particle density. At the same speed, the larger the number of particles, the more information they contain and the longer the computation time required. The proposed hybrid algorithm needed 20% less computing time than the rainbow PIV algorithm, and the time required for reconstructing simulation datasets with different speeds was approximately the same.

Table 3. Effect of velocity value and particle density on reconstruction time.

Speed (pixels·s^{-1})	Time (s)					
	Method	Num100	Num200	Num300	Num400	Num500
1	Rainbow PIV	485	533	565	599	615
	Proposed	398	432	444	461	465
2	Rainbow PIV	495	550	590	620	626
	Proposed	404	457	475	484	482
3	Rainbow PIV	479	551	581	619	623
	Proposed	385	444	455	482	492
4	Rainbow PIV	435	473	573	619	623
	Proposed	366	457	473	483	493
5	Rainbow PIV	512	545	561	599	606
	Proposed	415	445	454	487	485

4. Experiments and analysis

A fluid velocity measurement system was built based on the particle imaging principle and the experimental system requirements of 3D color PIV. Figure 6 shows a schematic diagram of the experimental system. A white light source was used to provide a stable white beam after collimation. The size of the beam was adjusted by the aperture. Then, the adjusted beam was filtered by a linear filter to obtain a color volume beam, and the particles spread uniformly in the sample pool were irradiated. The depth of the particles was encoded by the color of the light. The light of different colors reflected by the particles passed through the Fourier lens and converged on the camera in the focal plane. The camera recorded the movement of the particles and formed a color particle image of the particles moving in the area. The 3D velocity field was obtained by processing and analyzing the images captured at adjacent moments. This study used the open-source datasets provided by Xiong *et al.*[22] for real experimental analysis.

The structural similarity (SSIM) index can evaluate the reconstruction results of the two algorithms. The SSIM index is expressed as

$$\mathrm{SSIM}(\boldsymbol{T}_1,\boldsymbol{T}_2)=\frac{(2\mu_1\mu_2+C_1)(2\omega_{12}+C_2)}{(\mu_1^2+\mu_2^2+C_1)(\omega_1^2+\omega_2^2+C_2)}, \quad (10)$$

where $\boldsymbol{T}_1$ and $\boldsymbol{T}_2$ represent the reconstruction results by rainbow PIV and the proposed algorithm, respectively, μ_1 and μ_2 represent the average gray of $\boldsymbol{T}_1$ and $\boldsymbol{T}_2$, respectively, ω_{12} is the covariance of $\boldsymbol{T}_1$ and $\boldsymbol{T}_2$, ω_1^2 is the variance of $\boldsymbol{T}_1$, ω_2^2 is the variance of $\boldsymbol{T}_2$, and C_1 and C_2 are constants. The SSIM index ranges from 0 to 1 (0 means completely dissimilar and 1 means identical).

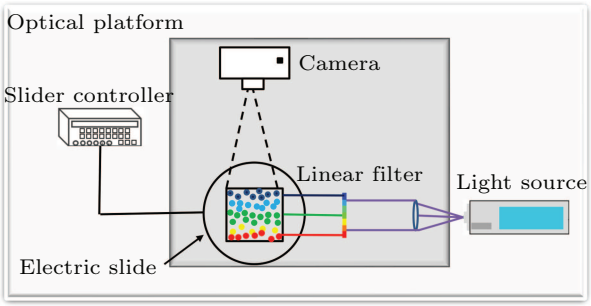


Fig. 6. The principle of the 3D color PIV experiment.

4.1. Single-vortex experiment

The size of the single-vortex experimental image captured by Xiong *et al.* was 3200 pixels×640 pixels. We selected a region of 960 pixels×576 pixels as the experimental dataset for more intuitive observation, as shown in Fig. 7.

Figure 8 shows the reconstructed 3D velocity field from the color particle images. Specifically, figure 8(a) shows the reconstruction result of rainbow PIV and figure 8(b) shows the result of the proposed hybrid algorithm.

It can be seen from the figure that the reconstruction results for these two 3D color PIV algorithms have similar flow patterns and, by calculation, the SSIM index of the two velocity fields is 0.9815. The reconstruction time of the rainbow

PIV algorithm was 375.447 s and that of the hybrid algorithm proposed in this paper was 279.628 s, a 25.52% improvement.

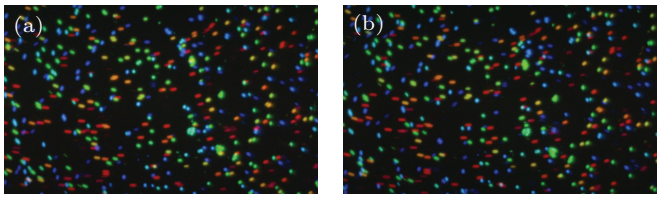


Fig. 7. Single-vortex experiment image pairs: (a) color particle image I_1 at time t_1, (b) color particle image I_2 at time t_2.

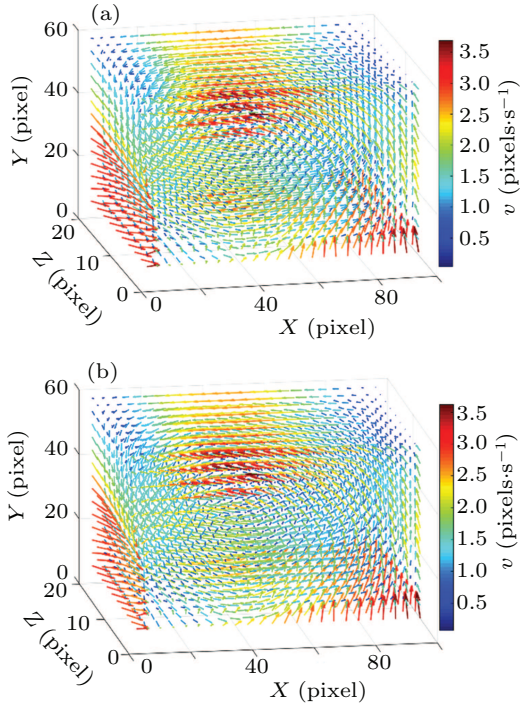


Fig. 8. Estimated velocity field of a single vortex experiment: (a) rainbow PIV, (b) proposed method.

4.2. Double-vortex experiment

In double-vortex dataset, an area of 960 pixels×576 pixels was also captured. The image pair is shown in Fig. 9.

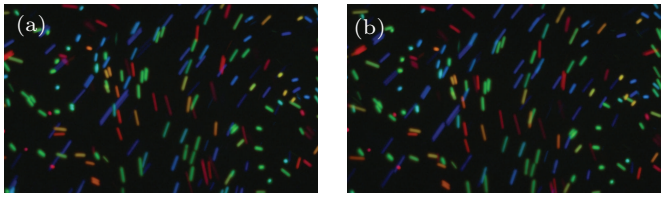


Fig. 9. Double-vortex experimental image pairs: (a) color particle image I_1 at time t_1, (b) color particle image I_2 at a time t_2.

Figure 10 indicates the reconstructed 3D velocity field from the color particle images.

Figure 10 shows that the flow trend of the fluid remained largely consistent. The SSIM index of the two velocity fields is 0.9872, verifying the correctness and accuracy of the proposed algorithm. The reconstruction times of the rainbow PIV algorithm and the proposed hybrid algorithm were 365.892 s and 278.826 s, respectively. The reconstruction speed of the proposed algorithm was 23.17% quicker.

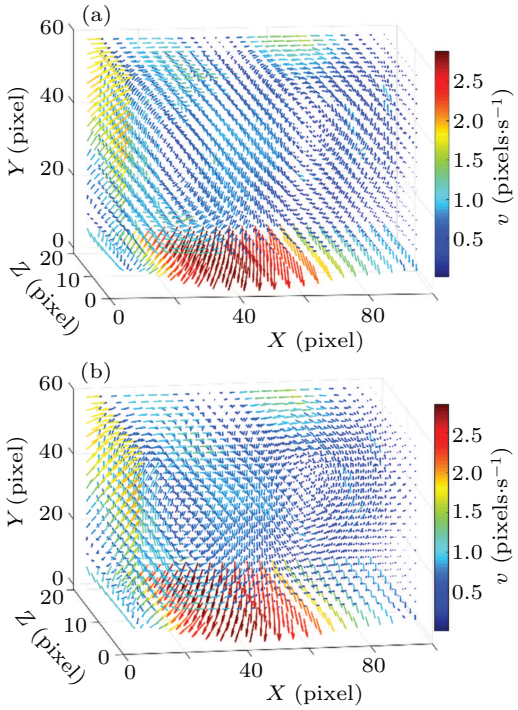


Fig. 10. Estimated velocity field of double-vortex experiment: (a) rainbow PIV, (b) proposed method.

4.3. Conclusion

This study proposes a 3D color PIV reconstruction algorithm based on a cross-correlation and optical flow method to improve the speed of velocity field reconstruction.

1) A single-vortex simulation experiment was performed, and the flow field was reconstructed using the rainbow PIV algorithm and the proposed hybrid algorithm. The AEPE, AAE and reconstruction time of the rainbow algorithm and the hybrid algorithm were compared. The results imply that the hybrid algorithm can perform the correct reconstruction and has roughly similar accuracy to the Rainbow PIV method. However, it was 20% quicker.

2) Vortex datasets with different velocity magnitudes and particle densities were simulated to discover the influence on the reconstruction performance.

3) The real data from single-vortex and double-vortex experiments were used to verify the practicability of the proposed algorithm. The SSIM indices for the two flow patterns were 0.9815 and 0.9872. The calculation speed of the proposed algorithm was approximately 24% quicker than that of the rainbow PIV method, which verifies better real-time performance.

Acknowledgement

Project supported by the National Natural Science Foundation of China (Grant Nos. 51874264 and 52076200).

References

[1] De León-Ruiz J E, Carvajal-Mariscal I, De La Cruz-ávila M, Klapp J and Guzmán J E V 2022 *Meas. Sci. Technol.* **33** 075406
[2] Zhang J H, Li B H, Wang Y F and Jiang N 2022 *Chin. Phys. B* **31** 074702
[3] Schlatter P and Örlü R 2010 *J. Fluid Mech.* **659** 116
[4] Etminan A, Muzychka Y S, Pope K and Baafour N K 2022 *Meas. Sci. Technol.* **33** 092002
[5] Lawson N J, Finnis M V, Tatum J A and Harrison G M 2005 *J. Visualization* **8** 261
[6] Kahler C J and Kompenhans J 2000 *Exp. Fluids* **29** S070
[7] Soloff S M, Adrian R J and Liu Z C 1997 *Meas. Sci. Technol.* **8** 1441
[8] Scarano F 2013 *Meas. Sci. Technol.* **24** 012001
[9] Yu T and Cai W W 2019 *Appl. Phys. Lett.* **115** 104104
[10] Zhang J Q, Qi H, Ji Y K, Ren Y T, He M J, Su M X and Cai X S 2022 *IEEE Trans. Instrum. Meas.* **71** 4500214
[11] Prasad A K 2000 *Exp. Fluids* **29** 103
[12] Calluaud D and David L 2004 *Exp. Fluids* **36** 53
[13] Van Doorne C W H and Westerweel J 2007 *Exp. Fluids* **42** 259
[14] Elsinga G E, Scarano F, Wieneke B and Van Oudheusden 2006 *Exp. Fluids* **41** 933
[15] De Silva C M, Baidya R and Marusic I 2013 *Meas. Sci. Technol.* **24** 024010
[16] Qu Q W, Cao Z, Xu L J, Liu C, Chang L Y and McCann H 2019 *Appl. Opt.* **58** 205
[17] Zhang J Q, Qi H, Jiang D H, He M J, Ren Y T, Su M X and Cai X S 2021 *Measurement* **175** 109107
[18] Xiong J, Aguirre-Pablo A A, Idoughi R, Thoroddsen S T and Heidrich W 2021 *Meas. Sci. Technol.* **32** 025401
[19] Zhu X Y, Zhang B, Li J and Xu C L 2020 *Opt. Commun.* **462** 125263
[20] Zhu X Y, Wu Z, Li J Zhang B and Xu C L 2021 *Opt. Lasers Eng.* **143** 106625
[21] Overbrueggen T, Klaas M, Bahl B and Schroeder W 2015 *SAE Int. J. Engines* **8** 1447
[22] Xiong J, Idoughi R, Aguirre-Pablo A A, Aljedaani A B, Dun X, Fu Q, Thoroddsen S T and Heidrich W 2017 *ACM Trans. Graph.* **36** 1
[23] Barbu I and Herzet C 2016 *Meas. Sci. Technol.* **27** 104002
[24] Zhang J Q, Qi H, Ren Y T, Su M X and Cai X S 2022 *Int. J. Heat Mass Tran* **188** 122660
[25] Glowinski R and Marroco A 1975 *R. A. I. R. O. Analyse Numérique* **9** 41
[26] Boyd S, Parikh N, Chu E, Peleato B and Eckstein J 2011 *Foundations and Trends in Machine Learning* **3** 1
[27] Ruhnau P and Schnörr C 2007 *Exp. Fluids* **42** 61
[28] Cai S Z, Xu C, Gao Q and Wei R J 2019 *Acta Aerodyn. Sin.* **37** 455